

# Phase diagram of a one-dimensional Ising model with an anomalous $\mathbb{Z}_2$ symmetry

Jin-Xiang Hao,<sup>1</sup> Wei Li,<sup>2,3,\*</sup> and Yang Qi<sup>1,4,†</sup>

<sup>1</sup>State Key Laboratory of Surface Physics and Department of Physics, Fudan University, Shanghai 200433, China

<sup>2</sup>CAS Key Laboratory of Theoretical Physics, Institute of Theoretical Physics, Chinese Academy of Sciences, Beijing 100190, China

<sup>3</sup>CAS Center of Excellence in Topological Quantum Computation,  
University of Chinese Academy of Sciences, Beijing 100190, China

<sup>4</sup>Collaborative Innovation Center of Advanced Microstructures, Nanjing 210093, China

Anomalous global symmetries, which can be realized on the boundary of symmetry-protected topological phases, bring new phases and phase transitions to condensed matter physics. In this work, we study a one-dimensional model with an anomalous  $\mathbb{Z}_2$  symmetry, using the density-matrix renormalization group method. Besides a symmetry-breaking ferromagnetic phase, we find a gapless phase described by the  $SU(2)_1$  conformal field theory, despite the existence of only discrete  $\mathbb{Z}_2$  symmetry in the Hamiltonian. The phase transition between the ferromagnetic phase and the gapless phase is continuous and has the same critical scaling as in the gapless phase. Our numerical finding is compatible of theoretical constraints on possible phases resulting from the symmetry anomaly.

## I. INTRODUCTION

Symmetry is an essential ingredient in the study of condensed matter physics. In traditional Landau paradigm [1], symmetries classify phases, and the spontaneous breaking of symmetries describes continuous phase transitions. In the last few decades, the discovery of topological states of matter, such as the intrinsic [2, 3] and symmetry-protected topological (SPT) orders [4–7] (including topological insulators and topological superconductors [8, 9]), greatly expands our understanding of phases and phase transitions. In particular, on the boundary of an SPT state, the symmetries are anomalous [10], meaning that the microscopic realization of the symmetries must be nonlocal. Such anomalous global symmetries can also be realized in a standalone system instead of on a boundary, if only the low-energy degrees of freedom (like half-integer spins) are considered [11]. Phases and phase transitions with anomalous global symmetries are different from their counterparts with anomaly-free symmetries. Most importantly, anomalous symmetries do not allow phases that are gapped, symmetric and trivial (without any intrinsic topological order). In general, anomalous symmetries lead to new phases, e.g., nontrivial gapless phases and phase transitions.

Although anomalous symmetries are generally realized as the boundary of a topological phase in one-higher dimension, numerical simulations using this realization is challenging because of the extra computational cost of simulating the bulk [12]. Therefore, it is desirable to study anomalous models without a bulk. Because of the topological nature of the anomaly, such models must be nonlocal: they either have a nonlocal Hamiltonian, or a nonlocal symmetry action. For the former approach, anomalous fermionic states violating the fermion-doubling theorem can be realized by the so-called SLAC-fermion Hamiltonian [13], which contains long-range hopping terms. For the latter approach, Chatterjee and Wen

[14] introduces systematic ways to construct such nonlocal symmetry actions realizing certain anomalies, and such models with anomalous  $\mathbb{Z}_2 \times \mathbb{Z}_2$  symmetry and  $S_3$  symmetry are used to simulate phases and phase transitions with anomalous symmetries without the bulk [15]. Comparing to the former approach, these models are easier to handle numerically because the Hamiltonian is still local. Therefore, this is a promising way to study phase and phase transitions with anomalous symmetries.

In this work, we study a one-dimensional (1d) spin model introduced in Ref. [14] with an anomalous  $\mathbb{Z}_2$  symmetry numerically, using the density-matrix renormalization group (DMRG) method. The anomaly indicates it is the boundary of a two-dimensional (2d)  $\mathbb{Z}_2$  SPT state. Therefore, it does not have a trivial paramagnetic phase, which is gapped and symmetric. Through tuning the coupling constants, we indeed find that the model realizes two phases: a symmetry-breaking ferromagnetic (FM) phase, which also appears in models with anomaly-free  $\mathbb{Z}_2$  symmetry, and a gapless phase described by the  $SU(2)_1$  [or the  $U(1)_2$ ] conformal field theory (CFT), which is known to describe the gapless symmetric edge state of the 2d  $\mathbb{Z}_2$ -SPT state. The overall phase diagram of this model closely resembles a spin-1/2 Heisenberg chain, although it only has a discrete  $\mathbb{Z}_2$  symmetry.

The rest of the paper is organized as follows. In Sec. II, we introduce the 1d model with an anomalous  $\mathbb{Z}_2$  symmetry proposed in Refs. [14, 16], and discuss possible phases compatible with the anomaly, using the boundary-bulk correspondence. In Sec. III, we give details of the DMRG method we use, and the physical quantities we compute. Section IV describes the numerical results we obtained, and Sec. V is devoted to the discussion.

## II. MODEL

In this work, we study the 1d lattice model introduced in Ref. [14], which has an anomalous  $\mathbb{Z}_2$  symmetry. The model

\* w.li@itp.ac.cn

† qiyang@fudan.edu.cn

Hamiltonian is the following,

$$H = -J_z \sum_{i=1}^L Z_i Z_{i+1} - h_1 \sum_{i=1}^L (X_i - Z_{i-1} X_i Z_{i+1}) - h_2 \sum_{i=1}^L Z_{i-1} (X_i + Z_{i-1} X_i Z_{i+1}), \quad (1)$$

where  $L$  is the number of sites, and  $X_i$  ( $Z_i$ ) is Pauli  $X$ ( $Z$ ) operator on the site  $i$ .

The Hamiltonian (1) has an anomalous  $\mathbb{Z}_2$  symmetry [14], described by the symmetry operator

$$W = \prod_i X_i \prod_i i^{\frac{-Z_i + Z_{i+1} + Z_i Z_{i+1} - 1}{2}}. \quad (2)$$

This is an anomalous non-on-site symmetry because it cannot be expressed as a product of local operators. In addition to flipping spins, the  $W$  operator adds a phase factor for each nearest-neighbor pair of spins: the phase factor is  $+1$  if the spins are  $|\uparrow\uparrow\rangle$ ,  $|\downarrow\downarrow\rangle$  or  $|\downarrow\uparrow\rangle$ , and  $-1$  if the spins are  $|\uparrow\downarrow\rangle$ . Therefore, the overall action of  $W$  is flipping all spins and adding a  $\pm 1$  phase if the total number of  $|\uparrow\downarrow\rangle$  domain walls is even (odd), respectively. Since only the  $|\uparrow\downarrow\rangle$  domain walls are counted,  $W$  only strictly satisfies the  $\mathbb{Z}_2$  algebra  $W^2 = 1$  if the boundary condition is periodic. However, the slight violation of  $W^2 = 1$  by other boundary conditions should have negligible effect in the thermodynamic limit, which is also confirmed by our DMRG simulation. Therefore, in the DMRG simulation, we still mostly use open boundary conditions because it reduces the bond dimensions needed in the simulation.

Two possible phases in this 1d model can be derived using the anomalous  $\mathbb{Z}_2$  symmetry and the boundary-bulk correspondence of SPT states. Because of the anomaly, this 1d model can be realized on the edge of a 2d nontrivial SPT state protected by the  $\mathbb{Z}_2$  symmetry, which is known as the Levin-Gu [17] or CZX state [5]. We then gauge the  $\mathbb{Z}_2$  symmetry in the 2d bulk, and turns the  $\mathbb{Z}_2$ -SPT state to a double-semion topological order. Phases of (2) then corresponds to edge states of the double-semion topological order.

First, gapped edge states of the double-semion topological order are classified by the anyon-condensation theory [18–20]. In the double-semion topological order, there are four anyons: the trivial anyon  $\mathbb{1}$ , the semion  $s$ , its mirror image  $s^*$ , and their bound state  $ss^*$ . The semions  $s$  and  $s^*$  has topological spins  $\pm \frac{1}{4}$  [21], respectively, and their bound state  $ss^*$  is a boson. Since there is only one (nontrivial) bosonic anyon, there is only one way of anyon condensation: condensing  $ss^*$ . This corresponds to the  $\mathbb{Z}_2$ -symmetry-breaking FM phase in model (2) (1) [16]. Therefore, there is no gapped PM phase in (2) (1).

Next, we study gapless edge states of the double-semion topological order. It is well known that the double-semion topological order can be viewed as a Kalmeyer-Laughlin chiral spin liquid (KL-CSL) [22] stacked with its mirror-reflection copy (the anyons in the KL-CSL are  $\mathbb{1}$  and  $s$ ), and one possible chiral edge state of the KL-CSL is the chiral  $SU(2)_1$  [or equivalently  $U(1)_2$ ] CFT [23, 24], where chiral means there is only left-moving fields. Its mirror copy

then gives another chiral CFT with only right-moving fields. Stacking the two chiral CFTs together, we see that one possible edge state of the double-semion topological order is a (nonchiral)  $SU(2)_1$  CFT. We notice that  $SU(2)_1$  CFT is only one of possible gapless edge states. In fact, using recent progresses in the correspondence between gapless edges and bulk topological orders [25] and between anomalous edge CFT and bulk SPTs [26, 27], one can see that not only the  $SU(2)_1$  CFT, but infinitely many other gapless states can be realized on the boundary of double-semion topological order or  $\mathbb{Z}_2$ -SPT state. Among them,  $SU(2)_1$  is the simplest and most likely to be realized in the lattice model (2) (1).

### III. NUMERICAL METHODS

We employ the DMRG method to simulate the model Eq. (1), with the ITensor library [28]. In the calculations, we set a maximum bond-dimension of 2000 that guarantees very well converged results, with truncation errors below  $10^{-10}$ .

The order parameter of the  $\mathbb{Z}_2$  symmetry in this model is the average magnetization per site  $m = \frac{1}{L} \sum_i Z_i$ , where  $Z_i$  is Pauli  $Z$  operator on the site  $i$  (this can still be used as the order parameter despite of the anomaly, because of the form of the “patch charge operator” in this model [14]). We use the binder ratio  $U$ ,

$$U = 1 - \frac{\langle m^4 \rangle}{3\langle m^2 \rangle^2} \quad (3)$$

to locate the phase transition point.

During our calculation, we find that if we set the parameter  $h_2$  to a relatively large value, the model will always be in the FM phase. On the other hand, when the parameter  $h_2 = 0$ , the model Hamiltonian (2) has the special property that the classical FM state is always an exact eigenstate. Consequently, this state will remain to be the exact ground state for  $h_1$  smaller than a critical value, and this special property may affect the phase transition. Thus, we set the parameter to a small but nonvanishing value  $h_2 = 0.3$  (while fixing  $J_z = 1$ ) in the following calculation.

To determine what type of the CFT this model belongs to, we need to compute the central charge, which is the main characteristic of CFT. We can obtain it from the entanglement entropy of the model. For a one dimensional quantum system with a length  $L$  and a periodic boundary condition, the entanglement entropy  $S_E$  should follow a linear scaling with the conformal distance  $l$  [29],

$$S_E = \frac{c}{3} \cdot \ln \left[ \frac{4(L+1)}{\pi} \sin \frac{\pi(2r+1)}{2(L+1)} \right] + const. = \frac{c}{3} \cdot \tilde{l} + const., \quad (4)$$

where  $r$  is the subsystem size and  $c$  is the central charge. We notice that the periodic boundary condition is often used for computing the central charge because it gives much better finite-size scaling behaviors than the open boundary condition, despite of the additional computational cost.

#### IV. RESULTS

As a first step, we draw the phase diagram of the model Eq. (1) from DMRG data. To this end, we fix  $J_z = 1$  and  $h_2 = 0.3$ , and calculate the order parameter  $\langle m \rangle$ , the susceptibility  $\chi = \frac{\partial \langle m \rangle}{\partial h_1}$ , and the binder ratio [see Eq. (3)] of the 1d quantum system as a function of the parameter  $h_1$  at different system sizes, as shown in Fig. 1. Here, we get the results in open boundary condition for speeding up the calculation, and it has no effect on the results. Fig. 1d shows the phase diagram of the system.

From Fig. 1a, we can see that the order parameter  $\langle m \rangle$  goes from finite values to zero as increasing the value of  $h_1$ . This indicates that the system undergoes a phase transition from an FM phase to a  $\mathbb{Z}_2$ -symmetric phase as increasing  $h_1$ . In fact, the FM phase with small  $h_1$  is smoothly connected to the point of  $h_1 = h_2 = 0$ , where the model reduces to the classical ferromagnetic Ising model. Next, we locate the phase transition point at  $h_{1c} \approx 0.75(3)$  from these measurements. First, the susceptibility  $\chi$  shows a sharp peak at  $h_1 = 0.73$  [30]. Additionally, Fig. 1c shows that the binder ratios of different system sizes also cross at  $h_1 = 0.78$ , and the smooth crossing indicates that the phase transition is continuous. Determining the precise location of binder-ratio crossing turns out to be difficult, due to the oscillating finite-size dependence explained in Appendix A. Comparing these two measurements, we put the transition point between 0.73 and 0.78, and leave the task of finding the precise location of the quantum critical point to future works.

In order to determine the phase with zero magnetization, we calculate the entanglement entropy  $S_E$  for the half subsystem size as a function of  $h_1$  at different system sizes, as shown in Fig. 1b. We can see that below the critical point  $h_{1c}$ , the value of  $S_E$  is zero, and beyond  $h_{1c}$ , the value of  $S_E$  varies with the system size  $L$ . Moreover, we compute the entanglement entropy  $S_E$  as a function of the subsystem size  $r$  for  $J_z = 1.0$ ,  $h_1 = 1.4$ ,  $h_2 = 0.3$ , and a fixed system size  $L = 80$  with the periodic boundary condition, and the results are shown in Fig. 2a (blue data). We find that the value of the entanglement entropy increases with the increase of  $r$ . These results indicate that the phase, with a vanishing order parameter for  $h_1 > h_{1c}$ , is a nontrivial gapless phase. This gapless phase can be described by a 1d CFT.

To determine the type of the CFT for the gapless phase, we compute the central charge of the CFT. According to Eq. (4), we plot the entanglement entropy  $S_E$  as a function of the conformal distance  $\tilde{l}$  (shown in Fig. 2a) to obtain the central charge of the system from the slope of the function. We can see that except for the first few data points due to the boundary effect, the expected linear dependence for the entanglement entropy is obtained as the conformal distance increases, and we extract the central charge  $c = 1$  from the slope of the linear dependence. Moreover, we calculate the entanglement entropy and the central charge of the system near the critical point (see Fig. 2b). The results indicate that the system at the critical point  $h_{1c}$  is also a  $c = 1$  CFT.

It is well known that a large class of CFTs with central

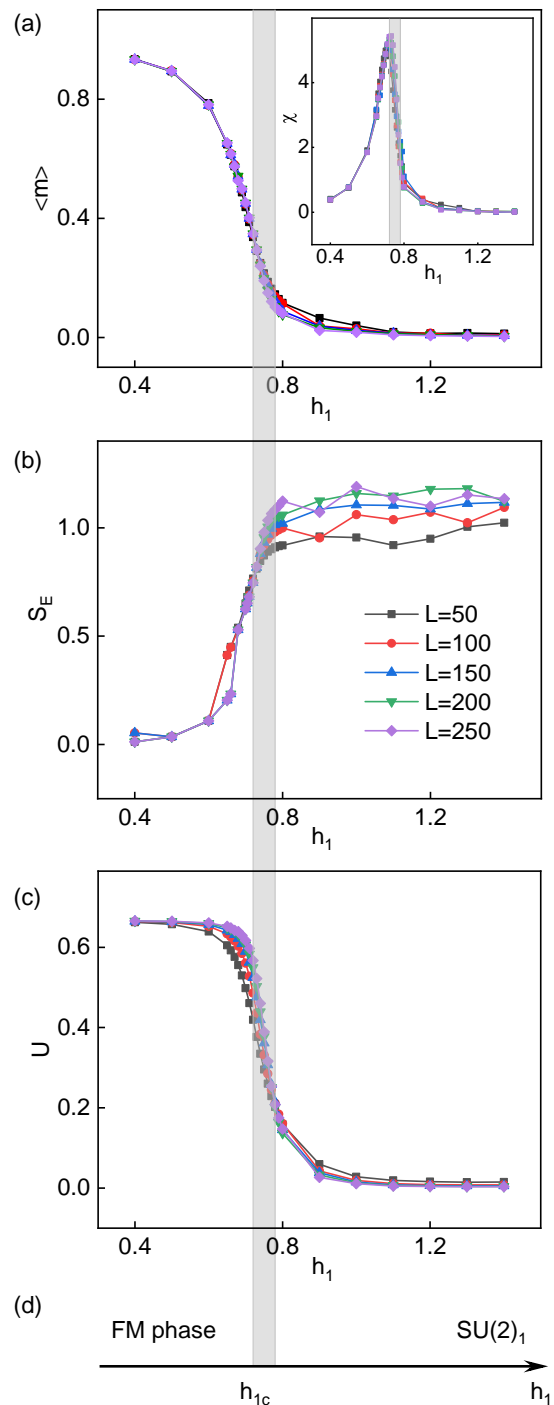


FIG. 1: (a) DMRG data for the order parameter (magnetization  $\langle m \rangle$ ) versus  $h_1$  for  $J_z = 1.0$  and  $h_2 = 0.3$ , with system sizes  $L = 50, L = 100, L = 150, L = 200$  and  $L = 250$  from top to bottom. The inset shows the corresponding  $\chi$  as a function of  $h_1$ . (b) The entanglement entropy  $S_E$  for the half subsystem size versus  $h_1$  in the same condition. (c) The binder ratio  $U$  of the system as a function of  $h_1$  in the same condition. The curves at different system sizes cross approximately at the critical  $h_c$ . We calculate (a), (b), and (c) at open boundary condition for efficiency, which is no effect on the results. (d) The phase diagram of the system for  $h_1$ . The grey line across all panels indicates the approximate location of the phase transition.

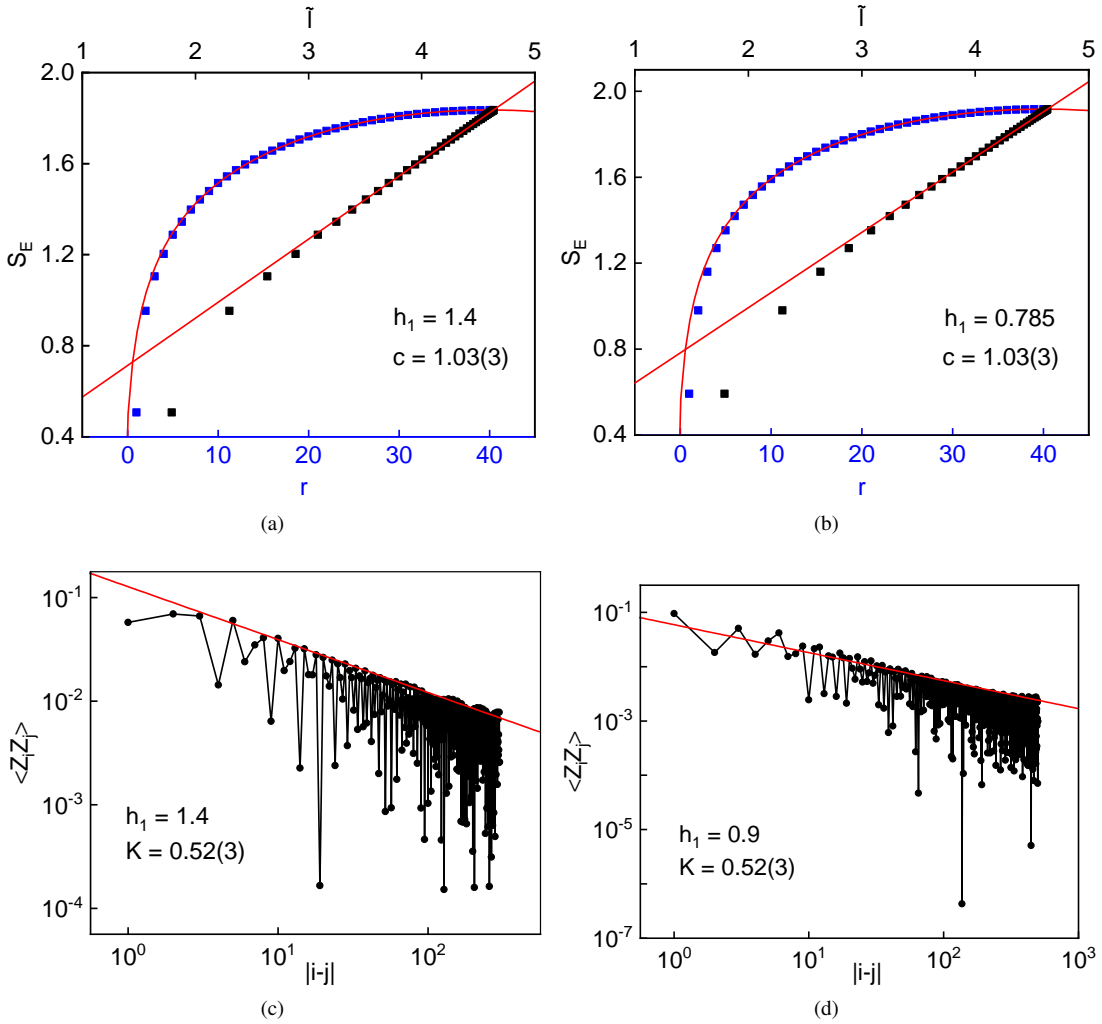


FIG. 2: (a) The blue data show that the entanglement entropy  $S_E$  of the system versus the subsystem size  $r$  for  $J_z = 1.0$ ,  $h_1 = 1.4$ ,  $h_2 = 0.3$ , and the system size  $L = 80$ . The black data show that the variation of entanglement entropy  $S_E$  of the system versus the conformal distance  $\tilde{l}$  for  $J_z = 1.0$ ,  $h_1 = 1.4$ ,  $h_2 = 0.3$ , and the system size  $L = 80$ . After discarding the first eight data due to the boundary effect, we can get the central charge  $c = 1$  by fitting the slope of the curve. We calculated the results in the periodic boundary condition. (b) The entanglement entropy of the system for  $h_1 = 0.785$ , near the critical point, in the same condition. (c) Variation of the correlation function  $\langle Z_i Z_j \rangle$  of the system versus the site distance  $|i - j|$  on a log-log scale, for  $J_z = 1.0$ ,  $h_1 = 1.4$ ,  $h_2 = 0.3$ , and the system size  $L = 600$  in the open boundary condition. We obtain the  $K = \frac{1}{2}$  from the slope of the data for the upper envelope. (d) The correlation function of the system near the critical point, for  $h_1 = 0.9$  and  $L = 1000$ , in the same condition, and we obtain  $K = \frac{1}{2}$ .

charge  $c = 1$ , including the  $SU(2)_1$  CFT discussed in Sec. II, is described by Luttinger liquids [31]. The Luttinger parameter is the main characteristic of Luttinger liquids, which we can extract from the power-law scaling of the correlation function  $\langle Z_i Z_j \rangle$ ,

$$\langle Z_i Z_j \rangle = |i - j|^{-K}, \quad (5)$$

where  $K$  is the Luttinger parameter.

We now turn to the calculation of the Luttinger parameter of the system. As shown in Fig. 2c, we plot, on a log-log scale, the correlation function  $\langle Z_i Z_j \rangle$  as a function of the site

distance  $|i - j|$ , for  $h_1 = 1.4$  and the system size  $L = 600$  in the open boundary condition. As a result, we obtain  $K = \frac{1}{2}$  by fitting the slope of the data for the upper envelope. We notice that in addition to the power-law decay, the correlation function also oscillates with distance, indicating that the critical  $\langle Z_i Z_j \rangle$  correlation occurs at a finite momentum. We leave a detailed investigation of this phenomenon to future works. We also compute the correlation function of the system near the critical point, for  $h_1 = 0.9$  and  $L = 1000$ , as shown in Fig. 2d. In this case, we also get the Luttinger parameter  $K = \frac{1}{2}$ . The result of  $K = \frac{1}{2}$  indicates that the CFT is  $SU(2)_1$ . In fact,

the scaling in (5) with  $K = \frac{1}{2}$  implies that the scaling dimension of the order parameter is  $\frac{1}{4}$ , consistent with the scaling dimension of the corresponding primary fields in the  $SU(2)_1$  CFT, and agrees with the topological spin of the semion excitation in the double-semion topological order. Therefore, our results suggests that the entire gapless phase of  $h_1 > h_{1c}$  is described by the  $SU(2)_1$  CFT. It is known that the phase transition from the  $SU(2)_1$  CFT to a gapped phase is of the Berezinskii-Kosterlitz-Thouless (BKT) type, which exhibits an exponentially long correlation length due to the essential singularity [32]. Therefore, it is challenging to study the scaling behavior near the BKT critical point, which we will leave to future works.

## V. DISCUSSION

In this work, we study the 1d model with an anomalous  $\mathbb{Z}_2$  symmetry introduced in Refs. [14, 16], using the DMRG method. We find that the model undergoes a phase transition from a FM order to a gapless phase when varying the parameter  $h_1$ , and we locate the critical point from the binder ratio of the  $\mathbb{Z}_2$  order parameter. In addition, we extract the central charge  $c = 1$  from the entanglement entropy scaling, and obtain Luttinger parameter  $K = \frac{1}{2}$  by fitting the exponent of the correlation function of the order parameter. According to these results, we determine that the gapless phase is described by the  $SU(2)_1$  [or  $U(1)_2$ ] CFT. Both the absence of a trivial PM phase and the CFT of the gapless phase agrees with theoretical expectations due to the anomaly.

We notice that the phase diagram we get in Fig. 1d resembles that of a spin- $\frac{1}{2}$  chain with nearest-neighbor and next-nearest-neighbor Heisenberg interactions (denoted by  $J_{1,2}$ , respectively), which is known as the Majumdar-Ghosh (MG) model [33]. The MG model also has a gapless phase described by the  $SU(2)_1$  CFT for  $J_1/J_2 < 0.2411$ , and a dimerized gapped phase with a spontaneous  $\mathbb{Z}_2$  symmetry breaking for  $J_1/J_2 > 0.2411$  [34]. From a renormalization-group analysis of the sine-Gordon model, it can be shown that the  $SU(2)$  symmetry enforces  $K = 1/2$ , and the power-law scaling of the spin-spin correlation remains the same until the phase-transition point [35]. This is consistent with our observations that  $c = 1$  at  $h_{1c}$ , and  $K = \frac{1}{2}$  at  $h_1 = 0.9$ , which is close to  $h_{1c}$ . In the MG model, the translation symmetry plays a similar role as the anomalous  $\mathbb{Z}_2$  symmetry in model (2), because the combination of translation and spin-rotation symmetry is anomalous [11]. It will be interesting to seek additional con-

nections between these two different models in future works.

Our results not only reveals an interesting phase diagram of the anomalous 1d model and its intriguing resemblance of 1d spin- $\frac{1}{2}$  chains, but also demonstrates the power of studying models with anomalous global symmetries with a nonlocal symmetry action and without an SPT bulk. We expect that systems with anomalous global symmetries, in both 1d and in higher dimensions, contain even richer phenomena than the traditional Landau-type symmetry-breaking phases and phase transitions, and models with nonlocal symmetry actions provide a viable way to study them.

## ACKNOWLEDGMENTS

This work was supported by National Natural Science Foundation of China (NSFC) through Grant Nos. 11874115, 12174068, 12222412, 11974036, 11834014, and 12047503.

## Appendix A: Oscillating size dependence of binder ratio

In this section, we discuss an oscillating finite-size dependence of binder ratio. This behavior affects the determination of binder-ratio crossing, which is used in the main text to locate the phase-transition point  $h_{1c}$ . In fact, although the binder ratio shows a crossing behavior in Fig. 1c in the main text, a zoom-in study of the plot in Fig. 3a exhibits irregular  $h_1$  dependences at different system sizes, and the curves do not cross at a single point.

To further investigate the size dependence of the binder ratio, in Fig. 3, we plot the system-size dependence of the binder ratio, at different values of  $h_1$ . The results show that when  $h_1 \geq h_{1c}$ , i.e. at the critical point or in the gapless phase, the binder ratio oscillates with  $L$ , with a period about 5-6. In contrast, the binder ratio in the FM phase varies smoothly with  $L$  without any oscillation. This is consistent with the oscillating  $\langle Z_i Z_j \rangle$  correlation function shown in Fig. 2(c)-(d). Therefore, we infer that the oscillating behavior in the binder ratio are caused by the finite-momentum spin correlation in the gapless phase: Because of the dominant spin correlation in the gapless phase occurs at a finite momentum, all thermodynamic quantities, including the binder ratio, exhibits an oscillating behavior depending whether the system size is commensurate with the period of the spin correlation or not. Furthermore, the oscillating behavior in Fig. 3b-c is responsible for the irregular  $h_1$  dependence in Fig. 3a, because the binder ratio also fluctuates with  $h_1$  at a fixed  $L$  as the location of peak and valley in Fig. 3b also shifts with  $h_c$ . Therefore, we will leave precise determination of phase transition point to future works.

- 
- [1] L. D. Landau, Zur theorie der phasenumwandlungen ii, Phys. Z. Sowjetunion **11**, 26 (1937).  
 [2] X. G. Wen and Q. Niu, Ground-state degeneracy of the fractional quantum hall states in the presence of a random potential and on high-genus riemann surfaces, Phys. Rev. B **41**, 9377 (1990).  
 [3] X. G. Wen, Topological orders in rigid states, Int. J. Mod. Phys.

- B **04**, 239 (1990).  
 [4] Z.-C. Gu and X.-G. Wen, Tensor-entanglement-filtering renormalization approach and symmetry-protected topological order, Phys. Rev. B **80**, 155131 (2009).  
 [5] X. Chen, Z.-X. Liu, and X.-G. Wen, Two-dimensional symmetry-protected topological orders and their protected gapless edge excitations, Phys. Rev. B **84**, 235141 (2011). The SPT

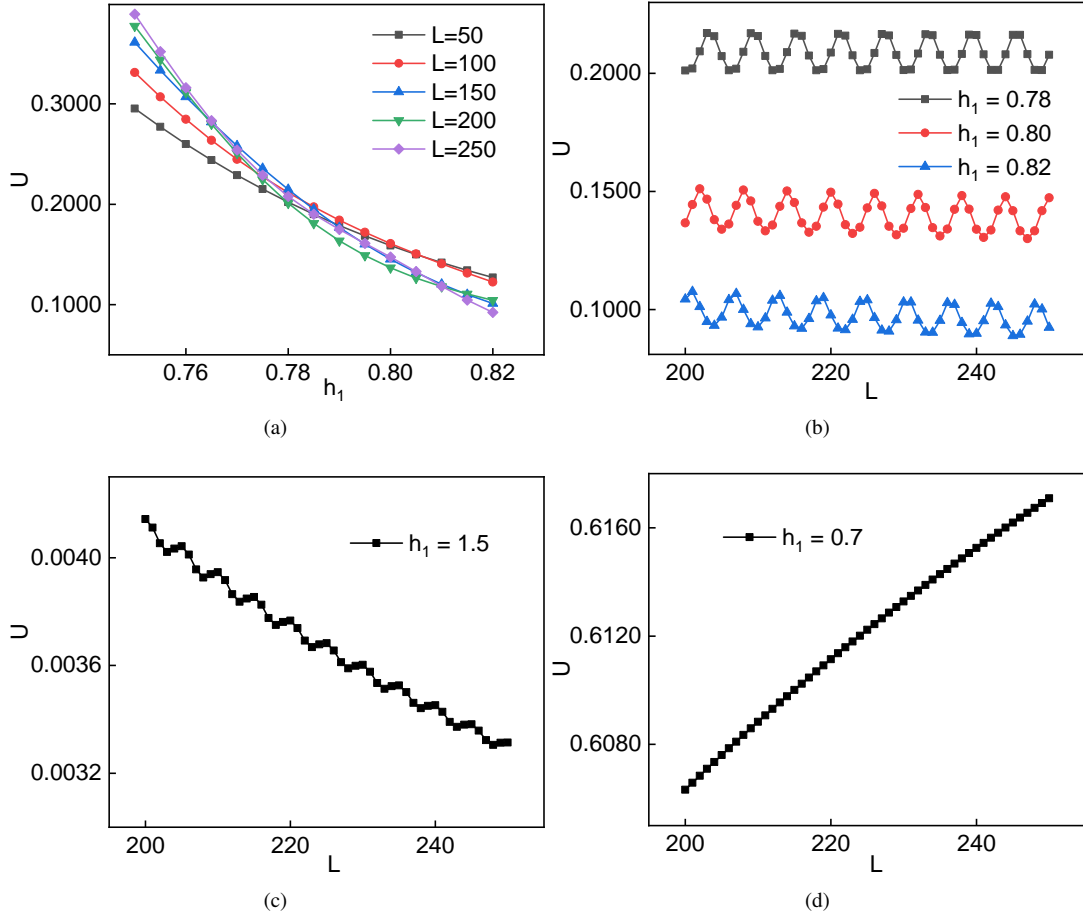


FIG. 3: Detailed study of  $L$  and  $h_1$  dependence of the binder ratio. (a) A zoom-in version of binder-ratio crossing shown in the main text. (b) Binder ratio as a function of system size, computed at values of  $h_1$  near the critical point. (c) Binder ratio as a function of system size, computed at  $h_1 = 1.5$ , which is in the gapless phase. (d) Binder ratio as a function of system size, computed at  $h_1 = 0.7$ , which is in the FM phase.

state described in this work is called the CZX state, because it is constructed using the control-X (CZX) quantum gate.

- [6] X. Chen, Z.-C. Gu, Z.-X. Liu, and X.-G. Wen, Symmetry-protected topological orders in interacting bosonic systems, *Science* **338**, 1604 (2012).
- [7] X. Chen, Z.-C. Gu, Z.-X. Liu, and X.-G. Wen, Symmetry protected topological orders and the group cohomology of their symmetry group, *Phys. Rev. B* **87**, 155114 (2013).
- [8] M. Z. Hasan and C. L. Kane, *Colloquium* : Topological insulators, *Rev. Mod. Phys.* **82**, 3045 (2010).
- [9] X.-L. Qi and S.-C. Zhang, Topological insulators and superconductors, *Rev. Mod. Phys.* **83**, 1057 (2011).
- [10] X.-G. Wen, Classifying gauge anomalies through symmetry-protected trivial orders and classifying gravitational anomalies through topological orders, *Phys. Rev. D* **88**, 045013 (2013).
- [11] M. Cheng, M. Zaletel, M. Barkeshli, A. Vishwanath, and P. Bonderson, Translational symmetry and microscopic constraints on symmetry-enriched topological phases: A view from the surface, *Phys. Rev. X* **6**, 041068 (2016).
- [12] Y.-C. Wang, C. Fang, M. Cheng, Y. Qi, and Z. Y. Meng, Topological spin liquid with symmetry-protected edge states, arXiv:1701.01552 [cond-mat.str-el].
- [13] S. D. Drell, M. Weinstein, and S. Yankielowicz, Strong-coupling field theories. ii. fermions and gauge fields on a lattice, *Phys. Rev. D* **14**, 1627 (1976). The model is named after the place it was invented: the Stanford Linear Accelerate Center (SLAC).
- [14] A. Chatterjee and X.-G. Wen, Algebra of local symmetric operators and braided fusion  $n$ -category—symmetry is a shadow of topological order, arXiv:2203.03596 [cond-mat.str-el].
- [15] A. Chatterjee and X.-G. Wen, Holographic theory for the emergence and the symmetry protection of gaplessness and for continuous phase transitions, arXiv:2205.06244 [cond-mat.str-el].
- [16] W. Ji and X.-G. Wen, Categorical symmetry and noninvertible anomaly in symmetry-breaking and topological phase transitions, *Phys. Rev. Research* **2**, 033417 (2020).
- [17] M. Levin and Z.-C. Gu, Braiding statistics approach to symmetry-protected topological phases, *Phys. Rev. B* **86**, 115109 (2012).
- [18] A. Kitaev and L. Kong, Models for gapped boundaries and domain walls, *Commun. Math. Phys.* **313**, 351 (2012).
- [19] L. Kong, Anyon condensation and tensor categories, *Nucl. Phys. B* **886**, 436 (2014).
- [20] F. Burnell, Anyon condensation and its applications, *Annu. Rev. Condens. Matter Phys.* **9**, 307 (2018).
- [21] Here, we express the topological spin as a fraction  $0 \leq S < 1$ , meaning that exchanging two identical anyons produces a statistical phase of  $e^{i2\pi S}$ .
- [22] V. Kalmeyer and R. B. Laughlin, Equivalence of the resonating-valence-bond and fractional quantum hall states, *Phys. Rev. Lett.* **59**, 2095 (1987).
- [23] X. G. Wen, Chiral luttinger liquid and the edge excitations in the fractional quantum hall states, *Phys. Rev. B* **41**, 12838 (1990).
- [24] B. Bauer, L. Cincio, B. Keller, M. Dolfi, G. Vidal, S. Trebst, and A. Ludwig, Chiral spin liquid and emergent anyons in a kagome lattice mott insulator, *Nat. Commun.* **5**, 5137 (2014).
- [25] L. Kong and H. Zheng, A mathematical theory of gapless edges of 2d topological orders. part I, *J. High Energy Phys.* **2020** (2), 150; A mathematical theory of gapless edges of 2d topological orders. part II, *Nucl. Phys. B* **966**, 115384 (2021).
- [26] T. Scaffidi and Z. Ringel, Wave functions of symmetry-protected topological phases from conformal field theories, *Phys. Rev. B* **93**, 115105 (2016).
- [27] M. Cheng and D. J. Williamson, Relative anomaly in  $(1+1)$ d rational conformal field theory, *Phys. Rev. Research* **2**, 043044 (2020).
- [28] M. Fishman, S. R. White, and E. M. Stoudenmire, The ITensor software library for tensor network calculations, arXiv:2007.14822 [cs.MS].
- [29] P. Calabrese and J. Cardy, Entanglement entropy and quantum field theory, *J. Stat. Mech.* **2004**, P06002 (2004).
- [30] The peak is not divergent as  $L$  increases, and this is consistent with the phase transition being of Berezinskii-Kosterlitz-Thouless type, which will be discussed later.
- [31] J. Luttinger, Fermi surface and some simple equilibrium properties of a system of interacting fermions, *Phys. Rev.* **119**, 1153 (1960).
- [32] C. Itzykson and J.-M. Drouffe, *Statistical Field Theory*, Cambridge Monographs on Mathematical Physics, Vol. 1 (Cambridge University Press, 1989).
- [33] C. K. Majumdar and D. K. Ghosh, On next-nearest-neighbor interaction in linear chain. I, *J. Math. Phys.* **10**, 1388 (1969); On next-nearest-neighbor interaction in linear chain. II, *J. Math. Phys.* **10**, 1399 (1969).
- [34] K. Okamoto and K. Nomura, Fluid-dimer critical point in  $s = 1/2$  antiferromagnetic heisenberg chain with next nearest neighbor interactions, *Phys. Lett. A* **169**, 433 (1992).
- [35] S. Sachdev, *Quantum Phase Transitions*, 2nd ed. (Cambridge University Press, 2011).